

Predictability and Uncertainty in Flow-Structure Interactions

D. Lucor and G.E. Karniadakis*
Center for Fluid Mechanics
Division of Applied Mathematics
Brown University

1 INTRODUCTION

Prediction of vortex induced vibrations (VIV) has been a semi-empirical discipline until recently. Most of the models employed in industrial applications (e.g., SHEAR7, VIVA, etc.) involve eigensolutions of the structure but the required flow input (e.g., lift coefficients, added mass, correlation length, etc.) is obtained empirically.

In the mid-1990s we initiated a research program (sponsored by ONR) in direct numerical simulation (DNS) of three-dimensional general flow-structure interactions in order to fill this gap. Our main focus has been on simulating VIV for flows past cylindrical flexible structures. We started at low Reynolds number (of the order of 100 to 200) and relatively small aspect ratio (of the order of 10). However, today based on new algorithms and faster parallel processors we simulate VIV at Reynolds number of the order of a few thousands and flexible cylinders with aspect ratio of the order of 1000. Although this range is still below the Reynolds numbers of industrial applications, from this new range extrapolations can be made, and indeed most of the predictions agree with experimental measurements quantitatively. Progress has also been made with respect to the type of structures we can simulate. Our initial efforts involved linear structures but more recent work has focused on non-linear structures with sag and vibrations in all three direction, i.e. including the axial direction.

In this review, we present some highlights of our work with emphasis on sheared inflow and non-linear structures. We also present our new path of research that attempts to model from first principles the various uncertainties associated with flow-structure interaction problems. This leads to a coupled system of stochastic differential equations for the flow and the structure, a computationally prohibitive task at first glance. However, we present a new approach to model stochasticity that involves extensions to the *polynomial chaos* method pioneered by Nobert Wiener in the late 1930s. The generalization of this approach that we have introduced could lead to a new generation of *non-sterilized* simulations of VIV, where uncertainties in flow conditions and structural properties or support are modeled explicitly.

2 VIV of FLEXIBLE CYLINDERS with SHEARED INFLOW

Following the work in [1, 2] of Direct Numerical Simulations (DNS) of uniform inflow past flexible cylinders subject to Vortex Induced Vibrations (VIV), we have focused on the physics of more complex flows corresponding to a wide range of inflow conditions. In particular, we have investigated different sheared (*linear* or *exponential*) inflows past long free flexible cylinders (aspect ratio greater than 500). We have also investigated oblique inflows with large angle of yaw past free rigid cylinders to access the validity of the

*Corresponding author, gk@cfm.brown.edu

Independence Principle [3].

In the simulations we employ the parallel three-dimensional version of the $\mathcal{N}\epsilon\kappa\mathcal{T}\alpha r$ code with a linear model for the structure and a Fourier expansion with a 3/2 de-aliasing rule in the longitudinal cable direction. A boundary-fitted coordinate system is employed similar to the simulations in [4], which has been validated against an Arbitrary Lagrangian Euler (ALE) formulation [5]. This is preferred for this part of our work as it provides adequate spatial resolution at a relatively low computational cost.

Figure 1 (right) shows an example of a linear sheared flow past a long flexible cylinder. We observe

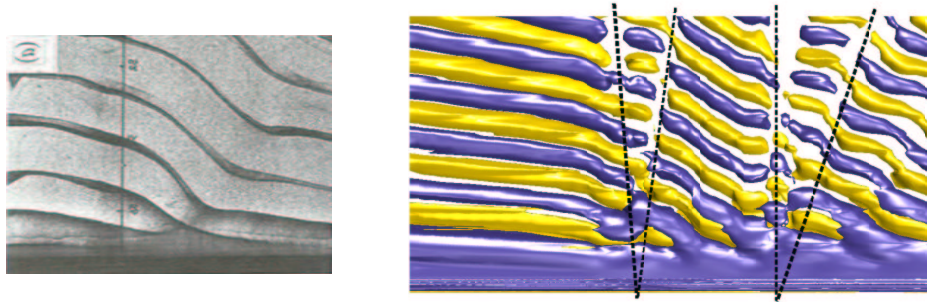


Figure 1: Experimental (left) vs Numerical (right) results. Left: Photograph of Vortex Dislocation at $Re=100$ for stationary cylinder using dye flow visualization (courtesy of Williamson [6]). Right: Isocontours of spanwise vorticity ($\omega_z = \pm 0.18$) and oblique fronts in the wake of a forced vibrating flexible cylinder at $Re=100$ with linear sheared inflow.

some vortex dislocations and vortex splits very similar to the ones obtained in [6] (see Figure 1: left). Strong vortex dislocations can result in substantial modulation of the forces on the body as it has been documented in [7].

In figure 2 (right), we present another example of complex flow physics successfully captured by DNS. In

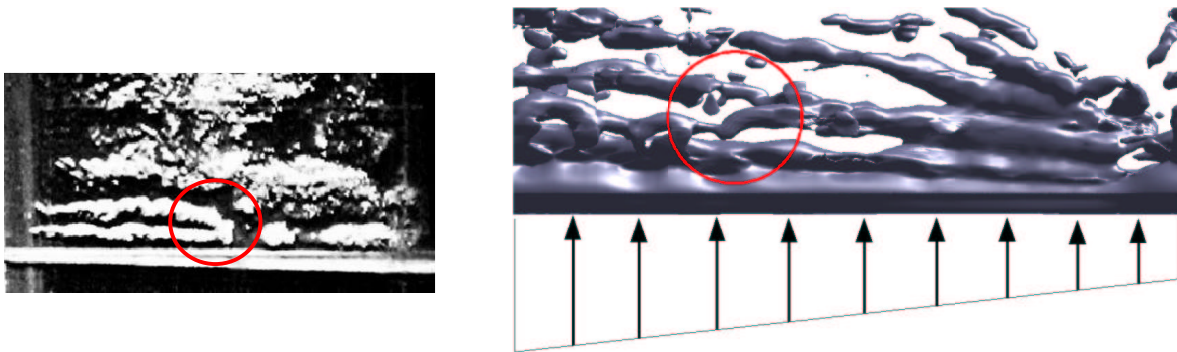


Figure 2: Experimental (left) vs Numerical (right) results. Left: Photograph of vortex *split* in the wake of a forced rigid tapered cylinder at $Re_{\bar{a}} = 400$ with uniform inflow using lead precipitation visualization (courtesy of Techet and *al.* [8]). Right: Isocontour of pressure ($p = -0.25$) in the wake of a forced rigid straight cylinder at $Re_{\bar{v}} = 400$ with sheared inflow.

this case, we properly resolve a vortex split that connects two vortical patterns (“2S” and “2P”) along a rigid cylinder forced to move in the cross-flow direction with a prescribed amplitude and frequency, see also [8]. In contrast to vortex dislocations, this *hybrid* mode is periodic and repeatable and the location of the vortex split remains stable.

3 FLOW-INDUCED VIBRATIONS of NON-LINEAR CABLES

Our next objective has been to bridge the gap that exists between studies of non-linear dynamic models for *general type* cables and DNS of flow past *simple* string/beam models. The former typically assumes a simplistic or empirical representation of excitation forces but provides very accurate models for the non-linear dynamic response of the cable allowing realistic description of both steel cables and synthetic cables with non-linear tension-strain relationship. The latter, on the other hand, assumes simple string/beam linear models but provides an accurate description of pressure and viscous forces, albeit (at present) in the low Reynolds number regime.

To this end, we have derived appropriate governing equations for non-linear cables and have developed a new formulation for the coupled flow-structure problem, see [9]. The structure is discretized using an explicit finite difference scheme with second-order accuracy in time and space while the flow is discretized using spectral/hp elements in the context of the arbitrary Lagrangian-Eulerian formulation (ALE). We have used effectively this new model to simulate large-scale industrial systems such as the lazy wave steel catenary riser (LWSCR), see below with details in [10].

3.1 Governing Equations for Non-Linear Cables

For *non-linear* cable, all three-directions are coupled and thus oscillations are excited both along the longitudinal (cable axis) direction as well as along the two transverse directions. We derive a unified formulation for non-linear cables in terms of a non-dimensional stretching parameter Δ .

Let us consider an infinitesimal segment of a stretched string in a “reference” position, which may not be in an equilibrium position. Let the arc length of the segment in this reference position be ds . We parameterize our string with respect to the arc length variable in the reference position, so that at any time t , we have arc length parameter $s(S,t)$ and an infinitesimal segment of length $ds(S,t)$. Let x, y and z be the two transverse and the longitudinal direction respectively, in an orthonormal coordinate frame for the string, then

$$ds^2 = dx^2 + dy^2 + dz^2 \Rightarrow \Delta = \frac{\partial s}{\partial S} = \sqrt{\left(\frac{\partial x}{\partial S}\right)^2 + \left(\frac{\partial y}{\partial S}\right)^2 + \left(\frac{\partial z}{\partial S}\right)^2}, \quad (1)$$

where Δ represents the length increase or decrease with respect to the reference position.

Let the tension in the string be $T(x, y, z)$ or $T(S, t)$ in terms of our fundamental parameterization. Given structural damping forces proportional to the string velocity (by a constant R), and external forces $\mathbf{F} = F_x|y|z$ in the three coordinate directions and the position vector $\mathbf{X} = [x \ y \ z]^T$, the fully non-linear equations are:

$$\frac{\partial}{\partial S} \left(\frac{T}{\Delta} \frac{\partial \mathbf{X}}{\partial S} \right) + \Delta [\mathbf{F}(S, t) - R \frac{\partial \mathbf{X}}{\partial t}] = m(S) \frac{\partial^2 \mathbf{X}}{\partial t^2}. \quad (2)$$

In the context of flow-structure interactions, F_x is drag, F_y is lift possibly with a gravitational body force $-m(S)g$, and F_z is the spanwise hydrodynamic force component.

The model for the tension derived for Poisson’s ratio $P = 1/2$ can be written as

$$T(s, t) = T(S) + EA(S) \left(1 - \frac{1}{\Delta} \right) = T_r + EA_r \left(1 - \frac{1}{\Delta} \right), \quad (3)$$

where $T(s, t)$ is expressed in terms of the tension in the reference position $T(S)$ and of a stretching term $EA(S) \left(1 - \frac{1}{\Delta} \right)$. When the reference position is that of a straight stretched (uniform in radius) string, we can rewrite the equation (see third part of equation (3)) where both the tension in the reference position $T_r = EA_r \epsilon$ and the cross-sectional area in the reference position A_r are constant.

For the case of $P = 0$, the model for the tension takes the form:

$$T(s, t) = EA_0(\Delta(\epsilon(S) + 1) - 1) = \Delta[T_r + EA_r(1 - \frac{1}{\Delta})], \quad (4)$$

where the last equality in the above equation is valid in the case of a reference position being a straight stretched string with uniform radius. Therefore, the presence or not of the incompressibility assumption leads to two different models for the tension, i.e., equations (3) and (4) and a dependence of a different nature on the non-linear parameter Δ .

3.2 Discretization and ALE formulation

We consider here the incompressible Navier-Stokes equations in a time-dependent domain $\Omega(t)$:

$$u_{i,t} + u_j u_{i,j} = -(p\delta_{ij})_j + \nu u_{i,jj} + f_i \quad \text{in } \Omega(t) \quad \text{and} \quad u_{j,j} = 0 \quad \text{in } \Omega(t), \quad (5)$$

We follow a variational form of the momentum equation in order to formulate the Arbitrary Lagrangian Eulerian (ALE) method. We multiply the Navier-Stokes equations by test functions from $H^1[\Omega(t)]$ and integrate by parts. In order to define the appropriate reference system on which time-differentiation takes place, we employ Reynolds transport theorem and use the fact that the test function is following the material points; therefore, its time-derivative in that reference frame is zero. The final variational statement then becomes

$$\frac{d}{dt} \int_{\Omega(t)} v_i u_i d\mathbf{x} + \int_{\Omega(t)} [v_i(u_j - w_j)u_{i,j} - v_i u_i w_{j,j}] d\mathbf{x} = \int_{\Omega(t)} [v_{i,j} p \delta_{ij} - \nu v_{i,j} u_{i,j} + v_i f_i] d\mathbf{x}. \quad (6)$$

This is the ALE formulation of the momentum equation where w_j is an arbitrary velocity that describes the motion of the time-dependent domain. It reduces to the familiar Eulerian and Lagrangian form by setting $w_j = 0$ and $w_j = u_j$, respectively. Introducing the mass matrix $\mathbf{M} \equiv (\phi(z), \phi(z))$, the derivative matrix $\mathbf{D} \equiv (\phi, \phi_z)$, and the stiffness (Laplacian) matrix $\mathbf{L} \equiv (\phi_z, \phi_z)$, where $\phi(z)$ is a spectral trial basis, we rewrite equation (6) and the incompressibility condition in compact form:

$$\frac{d}{dt} (\mathbf{M} \mathbf{U}_i) + \mathbf{N}_i(\mathbf{U}, \mathbf{W}) = \mathbf{D}_i^T \mathbf{P} - \mathbf{L}_{ij} \mathbf{U}_j + \mathbf{F}_i \quad \text{and} \quad \mathbf{D}_i \mathbf{U}_i = 0 \quad (7)$$

where we denote the non-linear contributions by $\mathbf{N}(\mathbf{U}, \mathbf{W})$ with dependence on the flow velocity field \mathbf{U} and mesh velocity \mathbf{W} . The equation for the mesh velocity is defined based on the mesh coordinates from:

$$\frac{dX_i}{dt} = W_i \quad (8)$$

We discretize equations (7) and (8) in time using a splitting scheme and stiffly stable integration of third-order [11]. We then solve for time step (n+1) by first treating explicitly the non-linear and the mesh velocity terms, and next by treating the elliptic terms implicitly. The mesh velocity is, in general, arbitrary, and it can be specified explicitly or be obtained from a Laplace equation or based on graph theory for smoother meshes [12].

3.3 Flow Induced Vibration of a Lazy Wave Riser

We consider a problem involving a riser of complex shape, which is immersed in quiescent flow. Specifically, we simulate the sag-bend response of the so-called lazy wave steel catenary riser (LWSCR) subject to a tangential forced motion at one end. The objective is to determine if the LWSCR in the absence of ocean current will experience intermittent flow-induced vibrations, and whether the resulting hydro-elastic excitation consists of a standing or a traveling wave response.

Figure 3 (left) provides a 3D schematic of the lower part of the LWSCR static configuration with its

buoyant sleeve. The structural model that we use accounts for time- and space-dependent tension in the structure. It also accounts for variable linear density of the structure. We use the tension model corresponding to Poisson ratio $P = 1/2$ (see equation (3)) and the tension of the structure in the reference position is taken constant, and thus we have $T(S) = T_0$. The reference position is, in this case, a straight stretched cable with constant tension. However, the code has the capability to treat a case with variable reference tension $T(S)$.

Figure 3 (right) shows the variable tension in the structure. The plot shows six different configura-

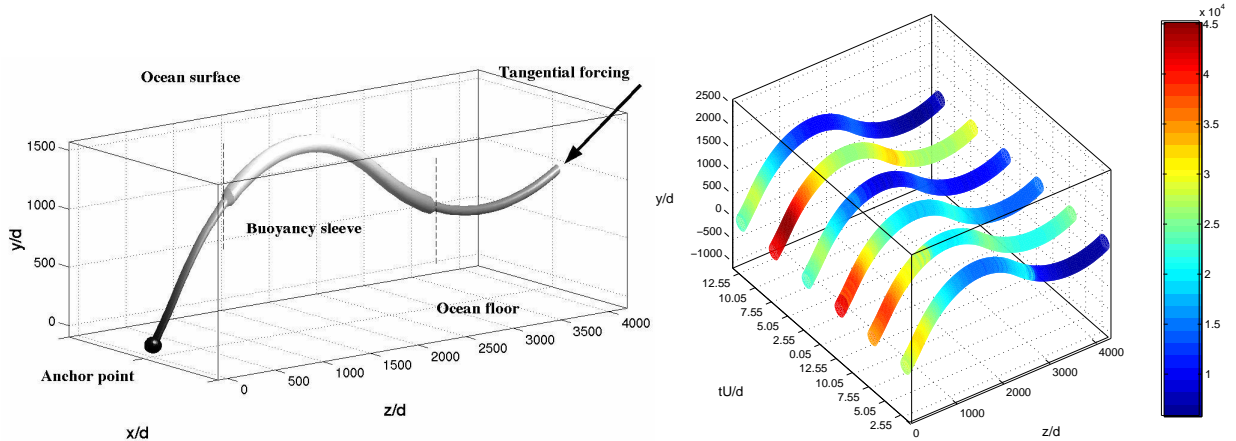


Figure 3: Left: LWSCR static configuration schematic (sag-bend part with enlarged body diameter). Right: Distribution of tension along the LWSCR sag-bend part at different times.

tions (corresponding to six different instants of time) and the corresponding magnitude of the tension is superimposed on the structure. The variation of tension, which is substantial, is larger in time than in space.

4 MODELING UNCERTAINTY

For flow-structure interactions the interest on stochastic modeling so far has primarily been on the dynamics of lumped systems, i.e., single- or two-degree-of-freedom second-order oscillators. The effect of the flow has been modeled via an interaction source term as either white noise or as a Gaussian distribution. However, non-Gaussian distribution behavior for the response has been documented in experiments. Here, we apply Wiener-Askey Polynomial Chaos method to solve stochastic coupled Navier-Stokes/structure system such as cylinders with random properties/boundary conditions subject to VIV.

The Wiener-Askey Polynomial Chaos expansion is a generalization of the original Polynomial Chaos. It is well suited to represent second-order random processes in terms of orthogonal polynomials. The expansion basis $\Psi_j(\boldsymbol{\xi}(\theta))$ is the complete polynomial basis from the Askey-scheme [13]. Using this type of representation, a general second-order random process takes the form:

$$u(\mathbf{x}, t; \theta) = \sum_{j=0}^P \hat{u}_j(\mathbf{x}, t) \Psi_j(\boldsymbol{\xi}(\theta)) \quad \text{with} \quad P = \frac{(n+p)!}{n!p!} - 1, \quad (9)$$

where we typically truncate the series up to $(P + 1)$ terms. The vector $\boldsymbol{\xi}(\theta)$ is the vector of independent random variables ξ_i , functions of the independent random variable θ . Since each type of polynomials from the Askey-scheme forms a complete basis in the Hilbert space determined by their corresponding support, we can expect each type of Wiener-Askey expansion to converge to any L_2 functional in the L_2 sense in the corresponding Hilbert functional space as a generalized result of Cameron-Martin theorem. The numerical procedure can be greatly simplified as most of the orthogonal polynomials from the Askey-scheme have weighting functions that take the form of probability function of certain types of random distributions.

4.1 Incompressible Navier-Stokes Equations

We consider laminar flow which can behave randomly subject to the randomness imposed by boundary conditions or random forcing. We expand the velocity and pressure in terms of the Polynomial Chaos expansion (see equation 9), substitute into the Navier-Stokes equations, and subsequently we project the obtained equations onto the random space spanned by the polynomial chaos basis. That is we take the inner product with each basis and use the orthogonality condition to simplify the equations. We obtain a discrete set of deterministic equations for the random modes. The random modes are only coupled through the convective terms.

4.2 Application to Flow-Structure Interactions

We consider the two-dimensional flow-structure interaction case of an elastically mounted circular cylinder with random structural parameters, subject to vortex-induced vibrations. We study the case of an unsteady flow in the laminar regime. The flow is computed using the procedure outlined above while the structural response (equation 10) of the moving cylinder is computed using a very similar procedure described in [13]. For the temporal discretization we use the implicit second-order Newmark scheme [14] for the equation

$$\ddot{\eta}(t, \theta) + c(\theta)\dot{\eta}(t, \theta) + k(\theta)\eta(t, \theta) = \mathbf{F}(t, \theta), \quad \eta(0) = \eta_0 \text{ and } \dot{\eta}(0) = \dot{\eta}_0 \quad (10)$$

We assume that the damping coefficient $c(\theta)$ and the spring factor $k(\theta)$ of the structure are both random variables. The free structure, excited by the vortex shedding of the flow follows a random response. Therefore, the position of the boundary of the cylinder becomes stochastic. This random boundary affects the flow domain, and consequently the flow itself becomes a stochastic process. The fluid forces on the cylinder are derived from the random flow velocity field and the random pressure field every time step.

$$\mathbf{F}(t, \theta) = \oint (-\Pi(t, \theta)\mathbf{n} + \frac{1}{Re}(\nabla\mathbf{u}(t, \theta) + \nabla\mathbf{u}(t, \theta)^T) \cdot \mathbf{n})ds. \quad (11)$$

To simplify the solution of the flow equations, we consider the initial coordinate system (x', y', t') and a coordinate system (x, y, t) attached to the moving cylinder. The stochastic flow equations are solved using a mapping approach based on the original deterministic mapping developed in [4]. This process maps the time-dependent and moving problem to a stationary and non-deforming one. Since the mapping involves the random cylinder velocity, it is a random process itself and is also represented by a polynomial chaos expansion.

4.3 Numerical Results

The Reynolds number is $Re = 100$, and the random parameters for the structure (see Equation 10) take the following form:

$$\begin{aligned} c &= \bar{c} + \sigma_c \xi_1(\theta) \\ k &= \bar{k} + \sigma_k \xi_2(\theta) \end{aligned} \quad (12)$$

where ξ_1 and ξ_2 are two independent random variables with zero mean, and σ_c and σ_k are the standard deviations of c and k .

We set $(\bar{c}, \sigma_c) = (0.1, 0.01)$, $(\bar{k}, \sigma_k) = (1.0, 0.2)$ while the initial conditions η_0 and $\dot{\eta}_0$ are set to 0. We note that there is a non-zero probability that the oscillator has a natural frequency $\omega_0 = \sqrt{k}$ matching the vortex shedding frequency of a fixed cylinder at this Reynolds number. Also, the system has two random dimensions ($n = 2$), and we use third-order Polynomial Chaos expansion ($p = 3$), which corresponds to a 10-term chaos expansion (i.e., $P + 1 = 10$).

Mean and *variance* solution for the cross-flow displacement and lift and drag coefficients are obtained using this method. Figure 4 shows instantaneous flood countours (gray scale) and countour lines (white color) of *rms* and *mean* of the vorticity field at $t = 600$ (non-dimensional time units, corresponding to more than 100 shedding cycles from the beginning of the simulation). Regions of the flow domain with high

uncertainty are the shear layers and the near-wake of the cylinder, which are of course the regions of utmost physical interest!

Figure 5 presents the pressure distribution on the cylinder surface at two instants of time within one

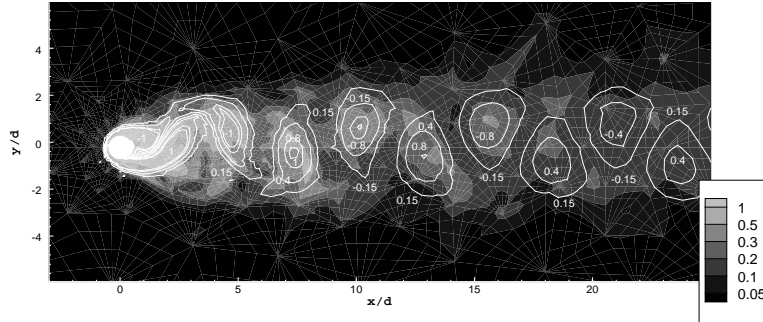


Figure 4: Instantaneous spatial distribution of *rms* (gray scale) and *mean* (white line) of vorticity.

shedding cycle of period T . Each plot shows an instantaneous polar view of the pressure distribution on the cylinder surface as well as the mean cross-flow position of the cylinder y/d at the corresponding time. The cylinder is represented by a black disk. The flow orientation is from left to right in each plot (angle $\theta = 180^\circ$: front stagnation point and $\theta = 0^\circ$: rear stagnation point). The deterministic pressure solution is represented by a dashed line while the stochastic solution is represented by a solid line (mean pressure solution) and a shaded area ('*error-bar*' region of the pressure solution). This region is centered around the mean curve and its span is two standard deviations (i.e., one *std* above and one *std* below the mean value). Both deterministic and stochastic pressure solutions take positive values around the front stagnation point. Noticeable differences exist between stochastic and deterministic solutions. In particular, temporal as well as spatial changes in the pressure variance (or '*error-bar*' region) can be seen. However, the deterministic signal remains, most of the time, inside the envelope of the stochastic solution.

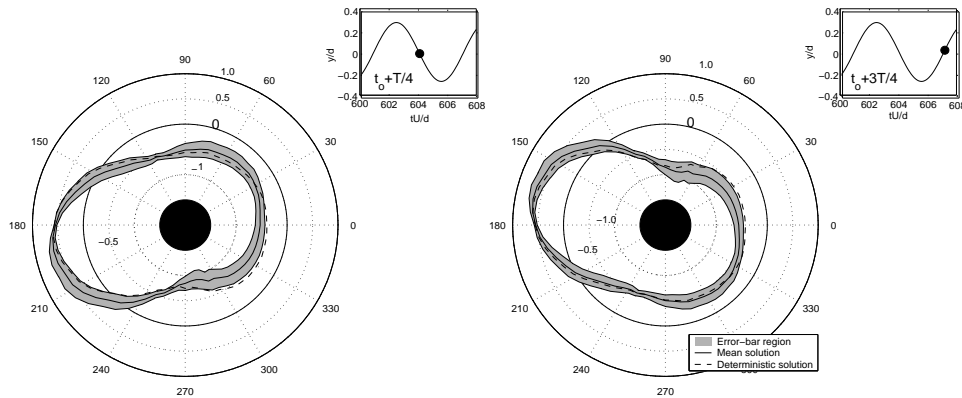


Figure 5: Polar plots of pressure distribution on the cylinder surface relative to the cylinder *mean* cross-flow position at different times. Deterministic pressure solution (dashed line); Stochastic pressure solution (solid line and shaded area).

Acknowledgements

We would like to thank the Office Of Naval Research for supporting this work (Dr. Thomas F. Swean). We are grateful to Prof. M.S. Triantafyllou for useful discussions related to this work. Computations were

performed on the Cray T3E at ERDC (Engineer Research and Development Center) and on the IBM SP3 at MHPCC (Maui High Performance Computing Center).

References

- [1] C. Evangelinos and G.E. Karniadakis. Dynamics and flow structures in the turbulent wake of rigid and flexible cylinders subject to vortex-induced vibrations. *Journal of Fluid Mechanics*, 400:91–124, 1999.
- [2] C. Evangelinos, D. Lucor, and G.E. Karniadakis. DNS-derived force distribution on flexible cylinders subject to VIV. *Journal of Fluids and Structures*, 14:429, 2000.
- [3] D. Lucor and G.E. Karniadakis. Effects of oblique inflow in vortex induced vibrations. Toulouse, France, April 8-12 2002. Proc. of IUTAM Symposium Unsteady Separated Flows.
- [4] D.J. Newman and G.E. Karniadakis. Simulations of flow past a freely vibrating cable. *J. Fluid Mechanics*, 344, 1997.
- [5] C. Evangelinos. *Parallel Simulations of VIV in Turbulent Flow: Linear and Non-Linear Models*. PhD thesis, Division of Applied Mathematics, Brown University, 1999.
- [6] C.H.K. Williamson. Oblique and parallel modes of vortex shedding in the wake of a circular cylinder at low Reynolds numbers. *Journal of Fluid Mechanics*, 206:579–627, 1989.
- [7] D. Lucor, L. Imas, and G.E. Karniadakis. Vortex dislocations and force distribution of long flexible cylinders subjected to sheared flows. *Journal of Fluids and Structures*, 15:641–650, 2001.
- [8] A. H. Techet, F. S. Hover, and M. S. Triantafyllou. Vortical patterns behind a tapered cylinder oscillating transversely to a uniform flow. *Journal of Fluid Mechanics*, 363:79–96, 1998.
- [9] C. Evangelinos, D. Lucor, C.-H. Su, and G.E. Karniadakis. Flow-induced vibrations of non-linear cables. Part 1: Models and algorithms. *International Journal for Numerical Methods in Engineering*, 55:to appear, 2002.
- [10] D. Lucor, C. Evangelinos, L. Imas, and G.E. Karniadakis. Flow-induced vibrations of non-linear cables. Part 2: Simulations. *International Journal for Numerical Methods in Engineering*, 55:to appear, 2002.
- [11] G.E. Karniadakis and S.J. Sherwin. *Spectral/hp Element Methods for CFD*. Oxford University Press, 1999.
- [12] R.M. Kirby, T.C.E. Warburton, S.J. Sherwin, A. Beskok, and G.E. Karniadakis. The NEKTAR code: Dynamic simulations without remeshing. In *Second International Conference on Computational Technologies for Fluid/Thermal/Chemical Systems with Industrial Applications, Boston, August 1-5, 1999*.
- [13] D. Xiu, D. Lucor, C.-H. Su, and G.E. Karniadakis. Stochastic modeling of flow-structure interactions using generalized polynomial chaos. *J. Fluid Eng.*, 124:51–59, 2002.
- [14] D. Lucor. *Stochastic Polynomial Chaos Simulations: Applications to Flow-Structure Interactions*. PhD thesis, Brown University, in progress.